

# Epitaxial Induced Plating Current-Collector Lasting Lifespan of Anode-Free Lithium Metal Battery

Liangdong Lin, Liumin Suo,\* Yong-sheng Hu, Hong Li, Xuejie Huang, and Liquan Chen

Anode-free designs can obtain the ultimate energy density of lithium metal batteries. However, without a continuous Li supply from the anode side, it is much more challenging to achieve high capacity retention with a competitive energy density. Here, the lifespan of an anode-free Li metal battery is prolonged by applying an epitaxial induced plating current-collector (E-Cu). The functional layer on E-Cu initiates Li storage by an alloying approach, forming an epitaxial induce layer, which exhibits speedy surface diffusion for of Li-ions, resulting in the block like epitaxial growth of Li. Moreover, this alloying process also promotes the formation of a LiF-rich solid electrolyte interphase (SEI), which is very useful for uniform Li plating. Due to the benefits of epitaxial Li plating and LiF-rich SEI, the initial coulombic efficiency of the E-Cu/Li asymmetric cell increases from 93.24 to 98.24%, and the capacity retention of anode-free NCM811/E-Cu pouch cell increases from 66 to 84% with a remarkable energy density of 420 Wh kg<sup>-1</sup> in the condition of limited electrolyte addition (E/C ratio of 2 g Ah<sup>-1</sup>). This strategy is promising in the development of high energy batteries in extending their lifespans.

again as next-generation advanced energy storage technologies.<sup>[3]</sup> Among all LMBs, anode-free lithium metal batteries (AF-LMBs) are regarded as the ultimate choice, prospectively exceeding 400 Wh kg<sup>-1</sup> at the cell level.<sup>[4]</sup> Except for its high energy density, the anode-free design also has potential advantages in cost and cell fabrication compared with traditional LIBs or Li-metal-based LMBs.<sup>[4,5]</sup> First, the cost of anode materials and the demand for electrolytes can reduce due to anode free, and the porous structure brought by the accumulation of anode material particles gone. Second, the fabrication of anode would be simplified with no need for applying the metallic Li in an extremely low-dew-point environment.

However, lithium metal anode (LMA) usually suffers from the low coulombic efficiency (CE) and fast capacity fading resulting from dendrite growth (dead

Li generation) during Li plating (stripping) and the continual side-reaction consuming by the formation of solid electrolyte interphase (SEI).<sup>[3]</sup> Thus, compared with the traditional LMBs, AF-LMBs are more challenging to achieve a long cycling life without Li compensation from the anode side. Recently, the CE of the state-of-art LMAs has been improved significantly above 99.5% by applying advanced electrolytes.<sup>[6]</sup> However, the CE is still not high enough for AF-LMBs to sustain their long cycling life.

Besides the electrolytes, the current-collector is another critical point to impact the reversibility of Li metal anode,<sup>[4c]</sup> which is a relatively new and challenging sub-field with a small amount of research mainly focusing on the surface modification on the current-collector substrate or the optimization of the underlying current-collector.<sup>[7]</sup> Moreover, the fabrications of these modified current-collectors, including plating,<sup>[7a]</sup> spin coating,<sup>[7b,e]</sup> CVD,<sup>[7d]</sup> and electrospinning,<sup>[7c]</sup> are complicated, whose mass loadings and thickness are hard to be controlled in the accepted level for the requirement of the energy density in cell level (Wh kg<sup>-1</sup> or Wh L<sup>-1</sup>).<sup>[7b,c,e]</sup> So far, the best performance of these strategies can enable an anode-free Cu@MLG/LFP cell to achieve capacity retention of 78% after 50 cycles.<sup>[7d]</sup>

Herein, an Epitaxial induced plating current-collector (E-Cu) with liquid metal (LM) coating layer is applied to extend the lifespan of AF-LMB by inducing efficient Li epitaxial plating along the current-collector. The functional LM coating layer on such current-collector, whose melting point is 6 °C, is composed of Ga, In, and Sn, with a mass ratio of 68.5:21.5:10.


## 1. Introduction

Lithium-ion batteries (LIBs) are rapidly expanding their applications to electric vehicles and electric energy storage after dominating the consumer electronics market.<sup>[1]</sup> However, their energy densities cannot keep up with the emerging demand restricted by Li-ion intercalation chemistry.<sup>[2]</sup> Under the circumstances, Li metal-based batteries (LMBs) arouse attention

Dr. L. Lin, Prof. L. Suo, Prof. Y.-s. Hu, Prof. H. Li, Prof. X. Huang, Prof. L. Chen  
Beijing Advanced Innovation Center for Materials Genome Engineering  
Key Laboratory for Renewable Energy  
Beijing Key Laboratory for New Energy Material and Devices  
Beijing National Laboratory for Condensed Matter Physics  
Institute of Physics  
Chinese Academy of Science  
Beijing 100190, China  
E-mail: suoliumin@iphy.ac.cn

Prof. L. Suo  
Center of Materials Science and Optoelectronics Engineering  
University of Chinese Academy of Sciences  
Beijing 100049, China

Prof. L. Suo  
Yangtze River Delta Physics Research Center Co. Ltd  
Liyang 213300, China

 The ORCID identification number(s) for the author(s) of this article can be found under <https://doi.org/10.1002/aenm.202003709>.

DOI: 10.1002/aenm.202003709

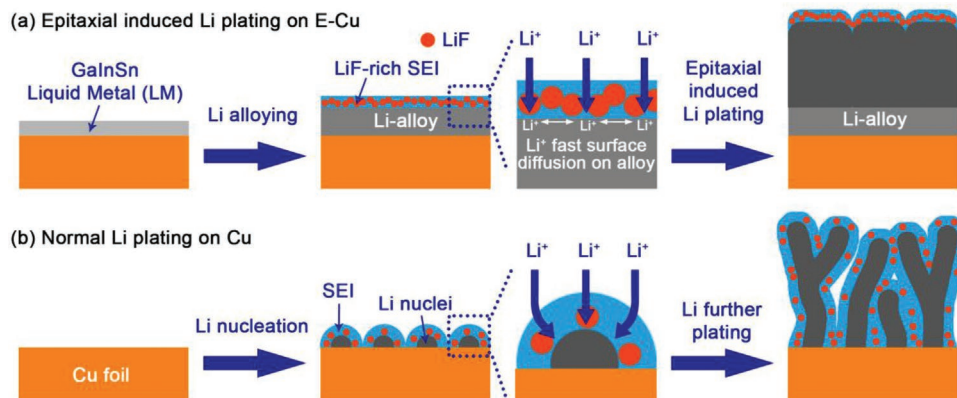


**Figure 1.** The concept of epitaxial induced Li plating. a) Illustrations of Li alloying and epitaxial induced plating behaviors on E-Cu. b) Illustrations of Li nucleation and plating behaviors on Cu.

Compared with pristine Cu current-collector, the functional LM layer initiating Li storage by alloying reaction, forming an epitaxial induce layer, as illustrated in **Figure 1a**. Moreover, benefiting from the lower LUMO energy of LiFSI than DME,<sup>[8]</sup> this alloying process with an operating potential around 0.75 V also promotes the formation of a LiF-rich SEI, which is favorable for uniform plating of Li.<sup>[5b,6a,c,d,9]</sup> The newly formed Ga, In, and Sn containing epitaxial induce layer exhibits speedy surface diffusion ability of Li-ions, and Li-ion can transfer flexibly after reaching the current-collector surface,<sup>[7a,10]</sup> thus effectively avoiding the plating of Li at a fixed site forming dendrite, resulting in the epitaxial growth of Li along the surface of inducing layer. The recently plated Li can maintain the original morphology of the epitaxial induce layer (**Figure 1a**) and continue to grow without undergoing a new nucleation process, which appears on Cu current-collector and is more likely to induce dendrite growth (**Figure 1b**). Benefiting from the epitaxial Li plating and LiF-rich SEI raised by the initial alloying process, the plating morphology of Li on our current-collector is very dense (**Figure 1a**) rather than porous dendrite (**Figure 1b**).

Besides, the fabrication of such a current-collector is quite simple, benefiting from the liquid nature of LM. Only a brush is needed to uniformly spread LM onto the surface of Cu foil with a mass loading of  $0.14 \text{ mg cm}^{-2}$ , which well retains the advantages of the anode-free design. This E-Cu with LM as a functional layer is denoted as E-Cu from now on. Using this E-Cu as the current-collector, the E-Cu/Li half-cell has a higher initial coulombic efficiency (ICE) of 98.24%. Moreover, the capacity retention of anode-free multi-layer pouch cell we assembled with high cathode mass loading ( $25 \text{ mg cm}^{-2}$ ) and limited electrolyte addition (E/C ratio of  $2 \text{ g Ah}^{-1}$ ) increased from 66 to 84% with a remarkable energy density of  $420 \text{ Wh kg}^{-1}$ , after replacing Cu current-collector with E-Cu.

## 2. Results and Discussions

### 2.1. Characterization of the E-Cu

To confirm that the coating of LM on Cu foil will not affect its thickness and weight much, scanning electron microscope

(SEM) images were collected. **Figure 2a,b**, and Figures S1 and S2, Supporting Information, show the surface SEM images of Cu and E-Cu, both of which are relatively flat overall. It can be observed that the unique morphology of Cu (**Figure 2a** and **Figure S1**, Supporting Information) disappears on E-Cu (**Figure 2b** and **Figure S2**, Supporting Information), proving that LM completely covers its surface. However, even coated with LM, the thickness of the current-collector does not change significantly (still  $\approx 6 \mu\text{m}$ ), as shown in the cross-sectional SEM images of Cu (**Figure 2c** and **Figure S3**, Supporting Information) and E-Cu (**Figure 2d** and **Figure S4**, Supporting Information) current-collectors. Furthermore, the mass loading of LM on Cu foil is weighted to be  $0.14 \text{ mg cm}^{-2}$  (only 2.5 wt% of  $6 \mu\text{m}$  Cu foil and its roughly estimated thickness is  $\approx 217 \text{ nm}$ ), not affecting the energy density of the cell much. **Figure 2e,f** show the Cu (**Figure 2e**) and Ga (**Figure 2f**) energy-dispersive X-ray spectroscopy (EDS) mapping of E-Cu cross-section (**Figure 2d**), confirming the cover of LM on Cu foil again. From the enlarged cross-sectional EDS mapping (**Figure S5**, Supporting Information), the overlapping of Cu and Ga can be observed, indicating the formation of CuGaInSn alloy at the interface. The formation of Cu alloy will lead to the solidification of LM at the interface, and such a solid-state interface is crucial for the stable adhesion of the LM layer because LM has a large surface tension, which makes it difficult to spread into a thin film spontaneously. The alloying of Cu and LM can effectively improve the wettability between them and realize the thin and stable coating of LM on the Cu foil surface. The chemical compositions of Cu foil before and after LM coating, were also characterized by X-ray photoelectron spectra (XPS), as shown in **Figure 2i-l**. LM consists of three elements: Ga, In, and Sn, whose signal can be observed on the LM coated Cu foil. Moreover, the Cu signal disappeared again, confirming that LM indeed totally cover the surface of the Cu foil.

### 2.2. Li Plating Morphologies on E-Cu and Cu Current-Collectors

Then, E-Cu and Cu were paired with Li plates as half-cells, and  $5 \text{ mAh cm}^{-2}$  Li plated onto Cu and E-Cu substrates with a current density of  $0.5 \text{ mA cm}^{-2}$  to observe the different nucleation

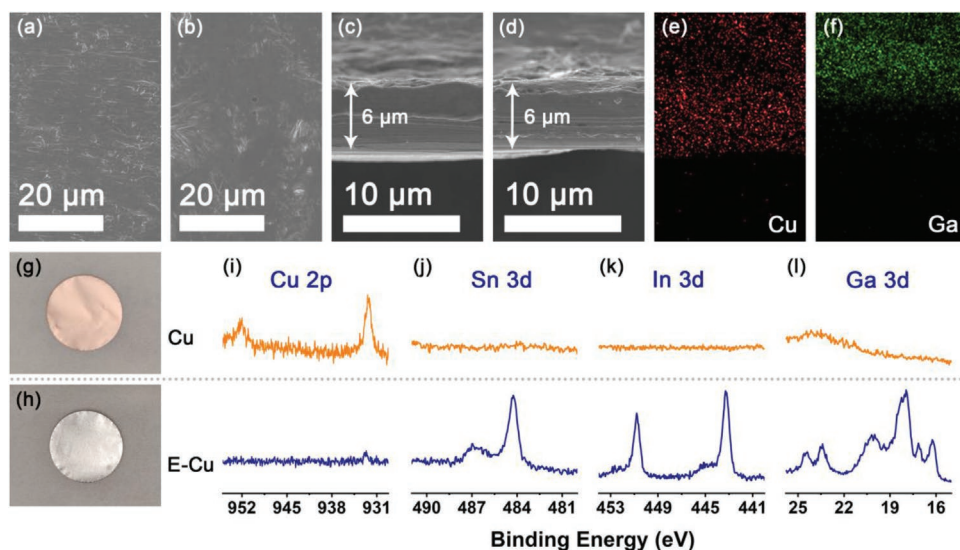


**Figure 2.** Morphology and composition of Cu and E-Cu current-collectors. SEM images of a) Cu and b) E-Cu current-collectors. Cross-sectional SEM images of c) Cu and d) E-Cu current-collectors. e) Cu and f) Ga EDS mapping of E-Cu cross-section. Digital photos of g) Cu and h) E-Cu current-collectors. i) Cu 2p, j) Sn 3d, k) In 3d, and l) Ga 3d XPS spectra of Cu (up) and E-Cu (down) current-collectors.

and growth behaviors of Li, as shown in **Figure 3**. Figure 3a–c shows the SEM images of Li plating on E-Cu. As expected, E-Cu shows significant advantages over Cu by providing a uniform and dense Li plating morphology (Figure 3a). While Li plating morphology on Cu is porous and dendrite like (Figure 3d), benefiting the generation of “dead Li” during Li stripping and the

side-reaction of Li with electrolyte.<sup>[11]</sup> To better understand the nucleation behavior of Li plating, the cross-sections of E-Cu and Cu current-collectors after Li plating were prepared by focused ion beam (FIB). As shown in Figure 3b, the plating of Li on E-Cu is indeed much denser, exhibiting a thickness of 37.5 μm, which is thinner than that of 46.7 μm on Cu (Figure 3e).

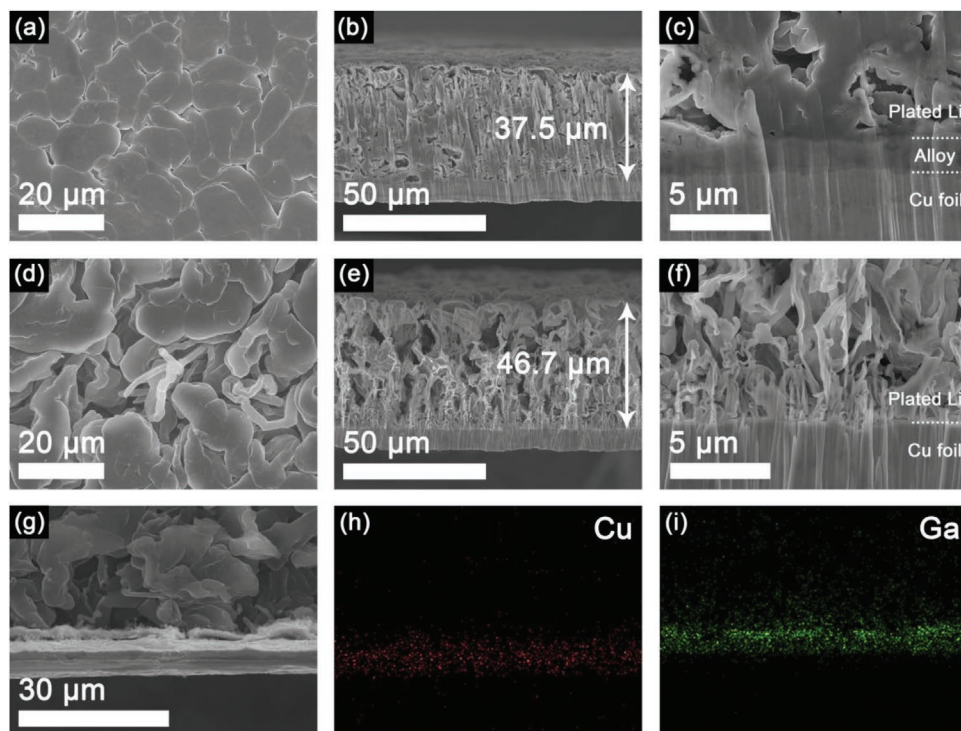


**Figure 3.** Li plating behaviors on E-Cu and Cu current-collectors. a) SEM image and b,c) cross-sectional SEM images of E-Cu current-collector after 5 mAh cm<sup>-2</sup> Li plating with a current density of 0.5 mA cm<sup>-2</sup>. d) SEM image and e,f) cross-sectional SEM images of Cu current-collector after 5 mAh cm<sup>-2</sup> Li plating with a current density of 0.5 mA cm<sup>-2</sup>. g) Cross-sectional SEM image and corresponding h) Cu and i) Ga EDS mapping of E-Cu current-collector after 5 mAh cm<sup>-2</sup> Li plating with a current density of 0.5 mA cm<sup>-2</sup>.

From the enlarged cross-sectional image of E-Cu, a prominent induce layer can be observed between Cu foil and plated Li (Figure 3c), which is a Li-alloy formed by the alloying reaction of Li-ions with LM at the beginning of the initial Li storage process. This newly formed Ga, In, and Sn containing epitaxial induce layer exhibits speedy surface diffusion ability of Li-ions,<sup>[7a,10]</sup> Li growth on E-Cu will not behave like that on Cu. On Cu foil, the nature of Li growth results in a large amount of Li nucleation, and Li tends to grow at these fixed sites (Li nuclei) because Li-ions cannot transfer rapidly after reaching the Li nuclei, which eventually leads to the 1D growth of Li forming high specific surface area dendrites (Figure 3f). While on E-Cu foil, Li-ions can transfer flexibly after reaching the epitaxial induce layer surface, and Li will grow uniformly around the E-Cu surface to achieve a 2D growth (Figure 3c). The initial plating of Li on E-Cu can inherit the original morphology of the induce layer and realize the so-called epitaxial growth without undergoing a new nucleation process, which appears on Cu and is more likely to induce dendrite growth (Figure 3f). Therefore, the dendritic high surface area morphology of Li plating on Cu will not appear on E-Cu. Instead, the bulk dense morphology can be observed. Moreover, the dense block like Li morphology is beneficial to reduce the side reactions of Li with electrolyte and the generation of “dead Li” thus effectively improving the stability of cell operation.<sup>[12]</sup> While the highly porous Li plating morphology on Cu is more likely to form isolated “dead Li” during cell operation, which seriously sacrifices precious Li resources and affects the lifespan of LMB.<sup>[13]</sup> Besides, it can be seen from the EDS mapping of E-Cu cross-section after Li plating (Figure 3g–i) that Ga is mainly distributed at the interface of Cu and plated Li, confirming that the primary function of E-Cu is to optimize the nucleation of Li plating and improve its initial growth behavior.

### 2.3. Characterization of SEI Components on E-Cu and Cu Current-Collectors

Notably, in addition to optimizing Li initial growth behavior, E-Cu can also affect the SEI by adjusting its composition, making it more conducive to efficient Li cycling. To illustrate this point, XPS spectra of E-Cu and Cu after 5 mAh cm<sup>-2</sup> Li plating were collected. Figure 4a–e shows the differences in XPS spectra between pristine E-Cu and Li plated E-Cu. The enhancement of O 1s and C 1s signals (Figure 4a,d) indicated the formation of SEI at the surface of plated Li, and the disappearance of Sn 3d, In 3d, and Ga 3d signals (Figure 4b,c,e) again confirmed that E-Cu mainly participates in the nucleation stage of Li plating. Although not involved in the growth process of Li plating, E-Cu can improve the composition of SEI during its formation, as shown in the XPS spectra of E-Cu and Cu after Li plating (Figure 4f–i). Two peaks could be derived from the high-resolution XPS spectra of F 1s (Figure 4f). The peak at 685 eV arises from LiF, and that at 689 eV comes from the C–F bond.<sup>[6a,d,9a,14]</sup> It is evident that the SEI formed on Cu contains more LiF, which is more conducive to the uniform Li plating.<sup>[5b,6a,c,d,9]</sup> Similarly, the contents of other inorganic components such as Li<sub>2</sub>CO<sub>3</sub> and Li<sub>2</sub>O (Figure 4g,h) in SEI formed on E-Cu are higher than those on Cu, while those of organic species such as C–F and C–O (Figure 4f,h), which come from the decomposition of electrolyte solvents, are much lower.<sup>[5b,6a,c,d,9]</sup> As we know, the compositions of SEI formed on different electrode materials with different electronic structures vary a lot.<sup>[15]</sup> The diversity in SEI between E-Cu and Cu can be attributed to the difference in LUMO levels of the electrolyte components and electrode potential during the formation of SEI.<sup>[8a,15f,16]</sup> According to the calculated LUMO energies reported in the previous literatures,<sup>[8]</sup> we find that the LUMO energy of DME (≈2.3 eV) is much higher than that of LiFSI

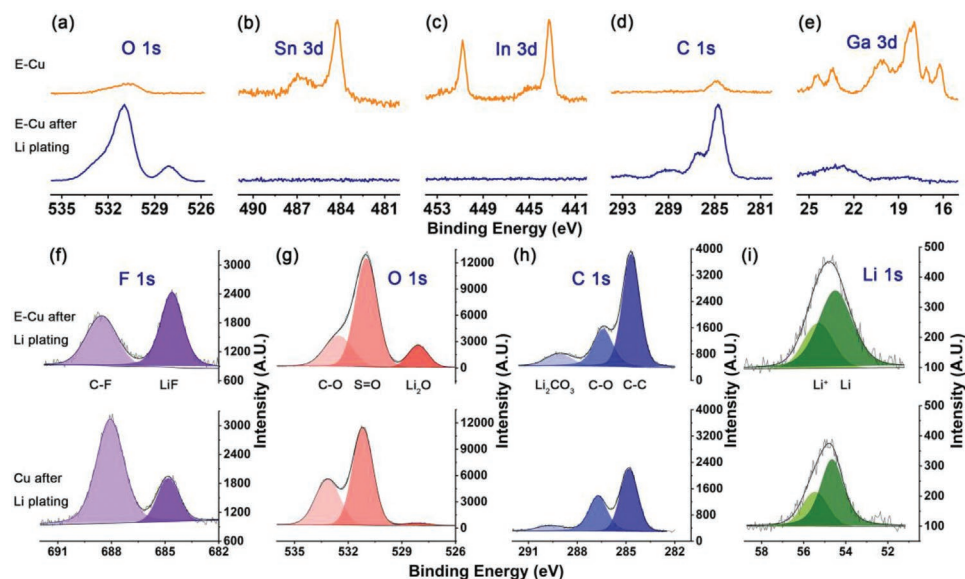


**Figure 4.** The influence of alloying on the formation of SEI. a) O 1s, b) Sn 3d, c) In 3d, d) C 1s, and e) G 3d XPS spectra of E-Cu before (up) and after (down) 5 mAh cm<sup>-2</sup> Li plating with a current density of 0.5 mA cm<sup>-2</sup>. f) F 1s, g) O 1s, h) C 1s, and i) Li 1s XPS spectra of E-Cu (up) and Cu (down) after 5 mAh cm<sup>-2</sup> Li plating with a current density of 0.5 mA cm<sup>-2</sup>.

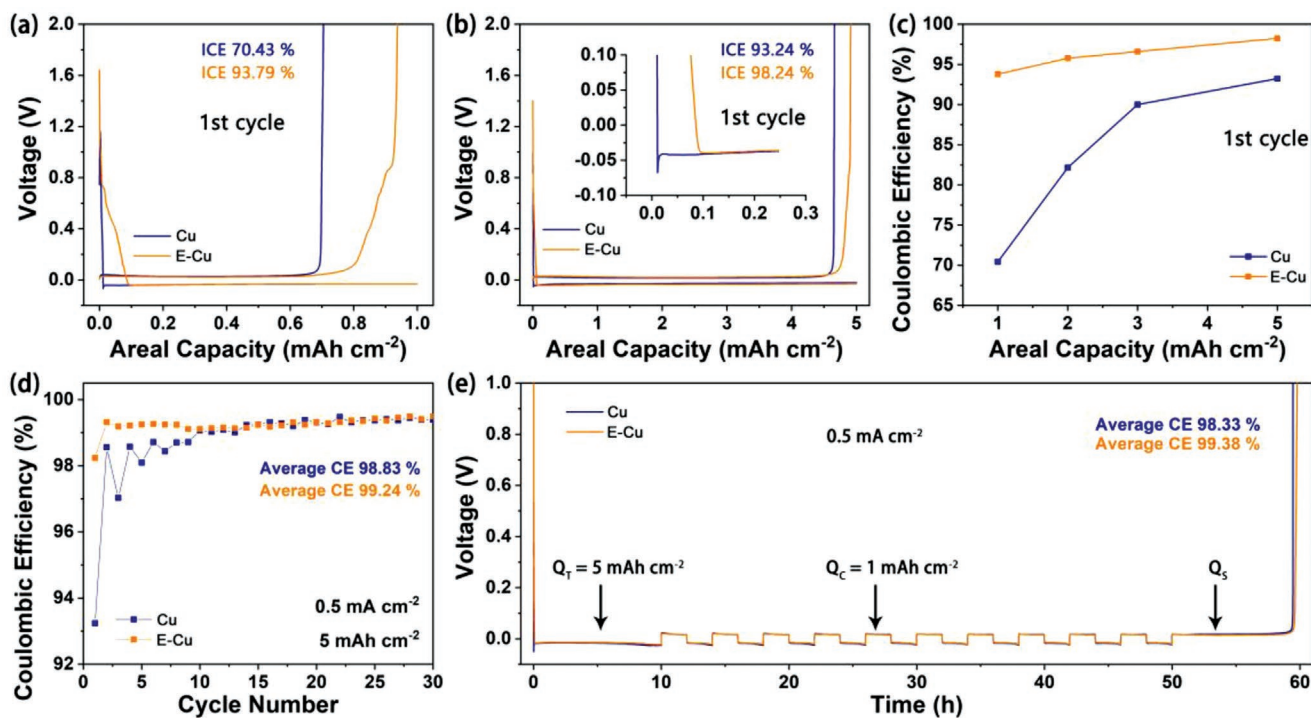


**Figure 5.** Advantages of E-Cu in Li utilization efficiency. Voltage profiles of Cu/Li and E-Cu/Li asymmetric cells cycling with capacities of a) 1 mAh cm<sup>-2</sup> and b) 5 mAh cm<sup>-2</sup> under 0.5 mA cm<sup>-2</sup>. c) ICEs of Cu/Li and E-Cu/Li asymmetric cells cycling with different capacities under 0.5 mA cm<sup>-2</sup>. d) Cycling performances of Cu/Li and E-Cu/Li asymmetric cells with a capacity of 5 mAh cm<sup>-2</sup> under 0.5 mA cm<sup>-2</sup>. e) The voltage versus time plots of Cu/Li and E-Cu/Li asymmetric cells under 0.5 mA cm<sup>-2</sup>.

( $\approx -1.5$  eV).<sup>[8b,d]</sup> So, when operating at a potential of 0.75 V on E-Cu, FSI<sup>-</sup> will decompose to form LiF in the SEI prior to DME due to its lower LUMO energy. Then, after the alloying reaction, the surface of the electrode has already been covered by LiF-rich SEI, which alleviates the further decomposition of DME. However, the potential on Cu instantly falls below 0 V, lower than the decomposition potentials of both DME and FSI<sup>-</sup>, DME and FSI<sup>-</sup> will decompose at the same time to form SEI, resulting in less LiF components in SEI. Benefiting from the dual optimization of nucleation and SEI by E-Cu during Li plating, the utilization efficiency of Li in Li-free anode is likely to be significantly improved.

#### 2.4. Electrochemical Performances of E-Cu in Asymmetric Cells

To verify the previous conjecture, asymmetric cells (E-Cu/Li or Cu/Li) cycled with different capacities under a current density of 0.5 mA cm<sup>-2</sup> (Figure 5). Figure 5a shows the E-Cu/Li and Cu/Li discharged into a fixed capacity of 1 mAh cm<sup>-2</sup> and then charged to 2 V to strip the Li off for the first cycle. Notably, E-Cu uses both alloying and plating approaches for reversible Li storage by providing an apparent alloying (de-alloying) plateau at the beginning of the discharge process (the end of the charging process). Benefiting from this alloying reaction, an epitaxial induce layer and a LiF-rich SEI formed at the surface of E-Cu. Therefore, E-Cu shows a significant advantage over Cu by giving a higher ICE (93.79% vs 70.43%) after 1 mAh cm<sup>-2</sup> Li plating/stripping. Similar phenomena were observed with

the increasing capacity, as shown in, Figure 5b and Figures S6 and S7, Supporting Information. When the capacity is up to 5 mAh cm<sup>-2</sup>, the ICE of E-Cu achieves 98.24% (Figure 5b). As shown in Figure 5c, with the increasing of areal capacity, the ICE of E-Cu always has advantages over Cu that remain in the following cycles, especially remarkable in the first ten cycles, where capacity loss is the most severe. (Figure 5d and Figures S8–S10, Supporting Information). Figure 5d shows that the CE of E-Cu reaches 99% at the 2nd cycle and continues to be higher than 99% in the following cycles, significantly outperforming Cu, whose CE cannot reach 99% until the 10th cycle. Based on these CEs, AF-LMB with E-Cu enables extending the cycling life from 10 cycles with Cu to more than 30 cycles with a capacity retention of 80%.

Aurbach CE tests,<sup>[17]</sup> which better evaluate Li cycling efficiency on plated Li substrate, were also carried out. To exclude the influence of the relatively low ICE on the measurement of average CE, a single Li plating/stripping cycle at a capacity of 5 mAh cm<sup>-2</sup> preconditioned on the E-Cu and Cu. After that, 5 mAh cm<sup>-2</sup> Li were plated onto these two substrates as Li reservoir (Q<sub>T</sub>). The cells then cycled with a fixed capacity of 1 mAh cm<sup>-2</sup> (Q<sub>C</sub>) for 10 cycles and finally stripped to 2 V (Q<sub>S</sub>), as shown in Figure 5e. The average CE calculates by Equation 1 where the first conditioning cycle was excluded.<sup>[17]</sup>

$$CE_{\text{avg}} = (nQ_C + Q_S) / (nQ_C + Q_T) \quad (1)$$

Based on the method, the Li average CE on E-Cu has 99.38%, much higher than that on Cu (98.33%). SEM images

of E-Cu and Cu after cycles were also collected to confirm the advantages of E-Cu over Cu. As shown in Figures S11–S14, Supporting Information, the amount of residual “dead Li” on E-Cu is significantly less than that on Cu, highlighting the high Li utilization efficiency on E-Cu. After 20 cycles, the differences in morphology become more apparent. A large amount of “dead Li” mixed in plated Li, and some cracks, was observed on Cu (Figures S15 and S16, Supporting Information). In contrast, the morphology of Li plating on E-Cu is much denser (Figures S17 and S18, Supporting Information). After stripping all the active Li off from the current collectors, the residual inactive components on Cu are much thicker than E-Cu (Figures S19–S22, Supporting Information), which again highlights the advantage of E-Cu. To verify the positive effect of the epitaxial induced plating without the LiF-rich SEI on Li anode, Cu/Li and E-Cu/Li asymmetric cells were tested with a standard 1 M LiTFSI + 0.1 M LiNO<sub>3</sub> in DOL/DME electrolyte. As shown in Figure S23, Supporting Information, the E-Cu/Li still shows higher CE than Cu/Li, indicating that the epitaxial induced plating on the GaInSn alloy layer is the main reason for the improvement in Li cycling. Since all the experimental results of E-Cu on Li utilization efficiency are quite encouraging, the E-Cu’s performances in full-cells are anticipated.

## 2.5. Electrochemical Performances of E-Cu in Pouch Cells

Furthermore, the 120 mAh level multi-layer anode-free pouch cells are assembled where NCM811 electrodes (25 mg cm<sup>-2</sup>,

30 \* 40 mm<sup>2</sup>) paired with E-Cu and Cu substrates (31 \* 41 mm<sup>2</sup>), respectively (Figure 6a and Figure S24, Tables S1 and S2, Supporting Information). Benefiting from the high Li utilization efficiency of E-Cu, NCM811/E-Cu can accumulate excess active Li on the anode side as Li reservoir after the first cycle, and work stably without capacity loss during the following 12 cycles, as shown in Figure 6b. This also can be confirmed by the CEs of NCM811/E-Cu, which always has advantages over NCM811/Cu throughout its cycling, especially remarkable in the first ten cycles, where the capacity loss in NCM811/Cu is the most severe. After depleting the Li reservoir on the anode side, NCM811/E-Cu also faces a linear capacity fading like NCM811/Cu dose. Even so, NCM811/E-Cu still outperformance NCM811/Cu in capacity retention with a higher Li inventory retention rate (LIRR, 99.65% vs 99.16%),<sup>[4c]</sup> which is a measure of the “average” loss in Li inventory per cycle and can be a reasonable value for comparison across different anode-free full cells. Based on the advantages mentioned above of E-Cu, NCM811/E-Cu has higher capacity retention of 84% than NCM811/Cu of 66% after 50 cycles (Figure 6b). Figure 6c shows the first cycle voltage profiles of NCM811/E-Cu and NCM811/Cu pouch cells. NCM811/E-Cu exhibits an apparent alloying plateau with a capacity of 3.5 mAh g<sup>-1</sup> (nearly 1.5% of the total capacity) and less voltage polarization at the beginning of the first charge (the inset of Figure 6c), which again proves the occurrence of the epitaxial growth of Li. Besides, NCM811/E-Cu shows a significant advantage over NCM811/Cu by giving a higher specific capacity of 200 mAh g<sup>-2</sup> and ICE of 85% (Figure 6c). Figure 6d shows the voltage profiles of NCM811/E-Cu pouch cells at the

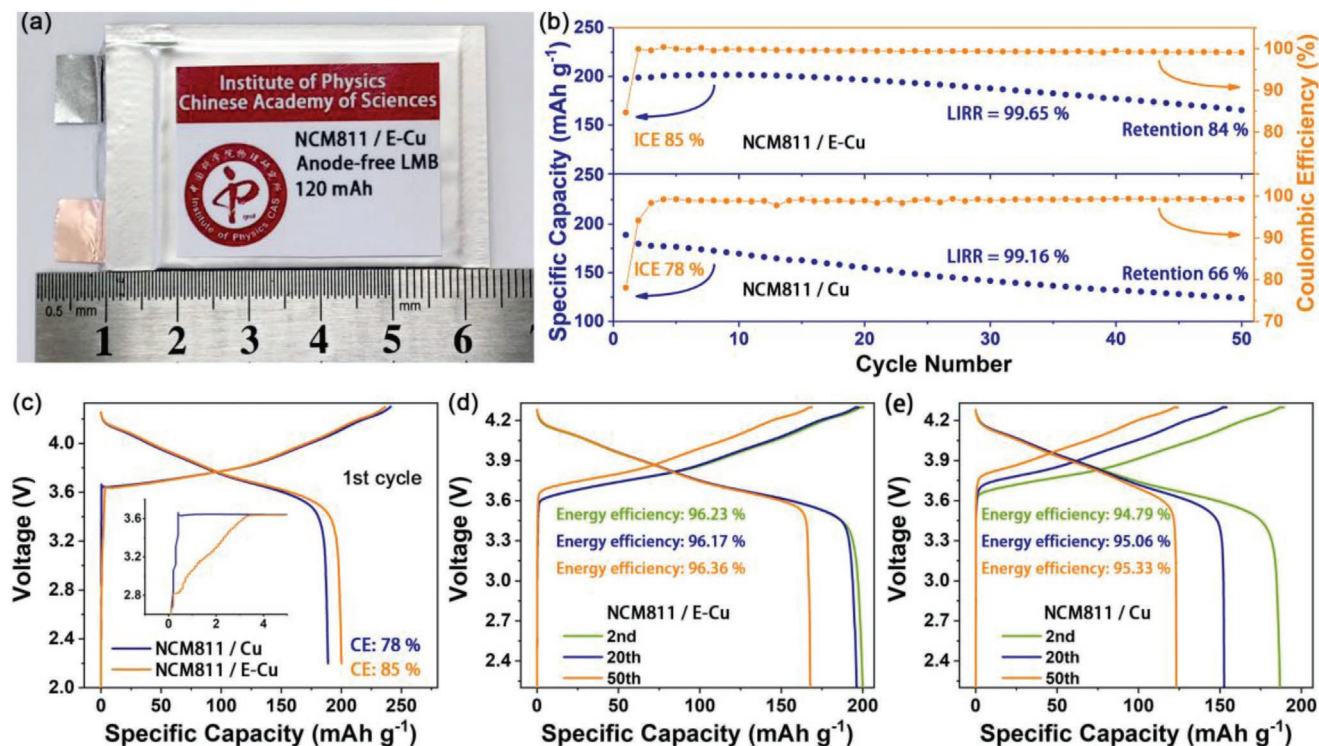


**Figure 6.** The demonstration of anode-free NCM811/E-Cu pouch cells. a) Digital photo of a 120 mAh level multi-layer anode-free pouch cell. b) Cycling performances of NCM811/E-Cu (up) and NCM811/Cu (down) pouch cells. c) Voltage profiles of NCM811/E-Cu and NCM811/Cu pouch cells. Voltage profiles of d) NCM811/E-Cu and e) NCM811/Cu pouch cells with different cycles.

2nd, 20th, and 50th cycles. Obviously, from the second cycle, the alloying reaction plateau at the charging process's initial disappears, confirm that the improved morphology of Li plating by the epitaxial induce layer is the decisive factor in further improvement on cycling performance of NCM811/E-Cu cell. Moreover, the NCM811/E-Cu cell has a quite high energy efficiency, higher than 96% (Figure 6d), which means lower energy loss during the energy storage/release, in line with the mainstream values of energy conservation. Even when the Li reservoir in the anode is exhausted and the cell capacity begins to decline from the end of discharge, the energy efficiency of the cell can still reach 96.36%. While the energy efficiency of the NCM811/Cu cell is lower than 96% throughout its cycling life with its capacity fading rapidly (Figure 6e). It is worth noting that, benefiting from the anode-free design, the energy density of this multi-layer NCM811/E-Cu cell core can reach 420 Wh kg<sup>-1</sup>, after excluding the weight of the packaging (Figure S25, Supporting Information).

### 3. Conclusions

In conclusion, we propose a new class of the LM coating current-collector for AF-LMB to extend its lifespan, enabling efficient Li epitaxial plating along the current-collector. In the first charge process, the functional layer on E-Cu uses both alloying and plating approaches for reversible Li storage. Benefiting from the initial Li alloying reaction, LiF-rich SEI, we successively manipulated the epitaxial Li growth on E-Cu. E-Cu/Li half-cell has a higher ICE of 98.24%. As a result, the capacity retention of AF-LMB (NCM811/E-Cu full-cell) increased to 84% with a remarkable energy density of 420 Wh kg<sup>-1</sup>, which would be possible to obtain if more advanced electrolytes could be introduced in the future. Meanwhile, the preparation of E-Cu is quite feasible, and the production of AF-LMB is compatible with the existing battery fabrication technology. All these above advantages make our strategy attractive to the further development of high energy density batteries.

### 4. Experimental Section

**Preparation of E-Cu Current-Collector:** E-Cu current-collector was fabricated by dropping 26  $\mu$ L LM (Ga:In:Sn = 68.5:21.5:10, Zhongxuan Liquid Metal Technology Co. Ltd.) onto Cu foil (30 \* 40 cm<sup>2</sup>) and spreading it evenly onto the surface of the Cu foil with a brush. The mass loading of LM on Cu foil is 0.14 mg cm<sup>-2</sup> on average. Then, the E-Cu current-collector or the Cu current-collector was punched into discs with a diameter of 16 mm for half-cells. Double-sided LM coated E-Cu current-collector was prepared by a similar process. Then, the double-sided LM coated E-Cu current-collector or the Cu current-collector was cut into 3.1 \* 4.1 cm<sup>2</sup> plates for multi-layer pouch cells.

**Preparation of NCM811 Cathode:** To fabricate NCM811 cathode, Li[Ni<sub>0.8</sub>Co<sub>0.1</sub>Mn<sub>0.1</sub>]<sub>2</sub>O<sub>7</sub> (NCM811, Ningbo Ronbay Lithium Battery Material Co., Ltd.), acetylene black (Alfa Aesar Co., Ltd.), and polyvinylidene fluoride (PVDF, Alfa Aesar Co., Ltd.) with a weight ratio of 96: 2: 2 in N-methyl pyrrolidinone (NMP, Sinopharm Chemical Reagent Co., Ltd.) were mixed in SK-300SII CE mixing machine (SHASHIN KAGAKU Co., Ltd.) for 20 min, producing a black slurry. Then, this slurry was spread on a clean Al foil by a doctor blade and dried at 60 °C for 12 h. The loaded foil was roll-pressed, and the mass of NCM811 in this electrode is 25 mg cm<sup>-2</sup> on average. Then the electrode was cut into 3 \* 4 cm<sup>2</sup> plates for multi-layer pouch cells.

**Preparation of Half-Cells:** Cu/Li and E-Cu/Li half-cells were assembled in CR2032-type coin cells using Cu foil or E-Cu foil as working electrodes and Li plate as counter electrodes, Celgard 3501 membrane as the separator, and 6 m bis(fluorosulfonyl)imide lithium (LiFSI) in 1,2-dimethoxyethane (DME) as the electrolyte. The as-prepared half-cells were tested with different capacities at a current density of 0.5 mA cm<sup>-2</sup> to evaluate their performance under different conditions.

**Preparation of Pouch Cells:** NCM811/Cu and NCM811/E-Cu pouch cells were assembled using NCM811 (30 \* 40 mm<sup>2</sup>) as the cathodes and Cu or E-Cu foil (31 \* 41 mm<sup>2</sup>) as anodes, Celgard 3501 membrane as the separator, 6 m LiFSI in DME as electrolyte (2 g Ah<sup>-1</sup>), and Al-plastic film as packaging.

**Characterizations:** XPS was taken using ESCALAB 250 XPS with monochromatic Al K $\alpha$  radiation. SEM images of the morphologies of Li plating on anodes were taken by Hitachi S-4800 field emission SEM, operated at 10 kV. All the samples were recovered from CR2032-type coin cell configuration after electrochemical cycling. The samples were washed by DME three times and then dried under vacuum for two hours before XPS or SEM measurement. A portable transfer vessel was used to process samples in glove-box and loaded into the XPS or SEM without exposure to air.

**Electrochemical Measurements:** For Cu/Li or E-Cu/Li half-cell CE cycling tests, cycling was done by plating 1, 2, 3, or 5 mAh cm<sup>-2</sup> of Li onto the Cu or LM electrode followed by stripping to 2V with a current density of 0.5 mA cm<sup>-2</sup>. The CE was calculated by dividing the stripping capacity by the plating capacity in a single cycle. And the average CE was calculated by dividing the total stripping capacity by the total plating capacity. For the Aurbach CE tests on plated Li, a standard protocol was followed: 1) perform one initial formation cycle with Li plating of 5 mAh cm<sup>-2</sup> on Cu or E-Cu under 0.5 mA cm<sup>-2</sup> current density and stripping to 2V; 2) plating 5 mAh cm<sup>-2</sup> Li on Cu or E-Cu under 0.5 mA cm<sup>-2</sup> as a Li reservoir; 3) repeatedly strip/plate Li of 1 mAh cm<sup>-2</sup> under 0.5 mA cm<sup>-2</sup> for 10 cycles; 4) strip all Li to 2V. The average CE was calculated by dividing the total stripping capacity by the total plating capacity. Galvanostatic cycling tests of NCM811/Cu or NCM811/E-Cu pouch cells were conducted within a voltage window of 2.2–4.3 V using battery testers (Wuhan Land, China, and Neware, China) at 25 °C. The pouch cells were charged to 4.3 V at 0.05 C and then discharged to 2.2 V at 0.2 C for the first formation cycle. After that, the pouch cells were charged to 4.3 V at 0.1 C and held at 4.3 V until the anodic current dropped below 0.05 C before discharged to 2.2 V at 0.2 C for the rest cycles.

### Supporting Information

Supporting Information is available from the Wiley Online Library or from the author.

### Acknowledgements

This work was supported by the National Key Technologies R&D Program, China (2018YFB0104400), and the China Postdoctoral Science Foundation (2019M660845).

### Conflict of Interest

The authors declare no conflict of interest.

### Data Availability Statement

The data that support the findings of this study are available from the corresponding author upon reasonable request.

## Keywords

anode-free, epitaxial plating, liquid metals, lithium metal anodes, lithium metal batteries

Received: November 27, 2020

Revised: December 26, 2020

Published online:

- [1] a) M. Armand, J. -M. Tarascon, *Nature* **2008**, 451, 652; b) B. Dunn, H. Kamath, J.-M. Tarascon, *Science* **2011**, 334, 928.
- [2] a) J. B. Goodenough, Y. Kim, *Chem. Mater.* **2010**, 22, 587; b) J. W. Choi, D. Aurbach, *Nat. Rev. Mater.* **2016**, 1, 16013.
- [3] a) D. Lin, Y. Liu, Y. Cui, *Nat. Nanotechnol.* **2017**, 12, 194; b) P. Albertus, S. Babinec, S. Litzelman, A. Newman, *Nat. Energy* **2018**, 3, 16.
- [4] a) J. Qian, B. D. Adams, J. Zheng, W. Xu, W. A. Henderson, J. Wang, M. E. Bowden, S. Xu, J. Hu, J.-G. Zhang, *Adv. Funct. Mater.* **2016**, 26, 7094; b) R. Weber, M. Genovese, A. J. Louli, S. Hames, C. Martin, I. G. Hill, J. R. Dahn, *Nat. Energy* **2019**, 4, 683; c) S. Nanda, A. Gupta, A. Manthiram, *Adv. Energy Mater.* **2020**, <https://doi.org/10.1002/aenm.202000804>.
- [5] a) A. J. Louli, A. Eldesoky, R. Weber, M. Genovese, M. Coon, J. deGooyer, Z. Deng, R. T. White, J. Lee, T. Rodgers, R. Petibon, S. Hy, S. J. H. Cheng, J. R. Dahn, *Nat. Energy* **2020**, 5, 693; b) Z. Yu, H. Wang, X. Kong, W. Huang, Y. Tsao, D. G. Mackanic, K. Wang, X. Wang, W. Huang, S. Choudhury, Y. Zheng, C. V. Amanchukwu, S. T. Hung, Y. Ma, E. G. Lomeli, J. Qin, Y. Cui, Z. Bao, *Nat. Energy* **2020**, 5, 526.
- [6] a) S. Chen, J. Zheng, D. Mei, K. S. Han, M. H. Engelhard, W. Zhao, W. Xu, J. Liu, J.-G. Zhang, *Adv. Mater.* **2018**, 30, 1706102; b) Y. Yang, D. M. Davies, Y. Yin, O. Borodin, J. Z. Lee, C. Fang, M. Olguin, Y. Zhang, E. S. Sablina, X. Wang, C. S. Rustomji, Y. S. Meng, *Joule* **2019**, 3, 1986; c) X. Cao, X. Ren, L. Zou, M. H. Engelhard, W. Huang, H. Wang, B. E. Matthews, H. Lee, C. Niu, B. W. Arey, Y. Cui, C. Wang, J. Xiao, J. Liu, W. Xu, J.-G. Zhang, *Nat. Energy* **2019**, 4, 796; d) L. Suo, W. Xue, M. Gobet, S. G. Greenbaum, C. Wang, Y. Chen, W. Yang, Y. Li, J. Li, *Proc. Natl. Acad. Sci. U. S. A.* **2018**, 115, 1156.
- [7] a) S. S. Zhang, X. Fan, C. Wang, *Electrochim. Acta* **2017**, 258, 1201; b) A. A. Assegie, J.-H. Cheng, L.-M. Kuo, W.-N. Su, B.-J. Hwang, *Nanoscale* **2018**, 10, 6125; c) L. H. Abrha, T. A. Zegeye, T. T. Hagos, H. Sutiono, T. M. Hagos, G. B. Berhe, C.-J. Huang, S.-K. Jjiang, W.-N. Su, Y.-W. Yang, B.-J. Hwang, *Electrochim. Acta* **2019**, 325, 134825; d) A. A. Assegie, C.-C. Chung, M.-C. Tsai, W.-N. Su, C.-W. Chen, B.-J. Hwang, *Nanoscale* **2019**, 11, 2710; e) Z. T. Wondimkun, T. T. Beyene, M. A. Weret, N. A. Sahalie, C.-J. Huang, B. Thirumalraj, B. A. Jote, D. Wang, W.-N. Su, C.-H. Wang, G. Brunklaus, M. Winter, B.-J. Hwang, *J. Power Sources* **2020**, 450, 227589.
- [8] a) X. Li, J. Zheng, X. Ren, M. H. Engelhard, W. Zhao, Q. Li, J.-G. Zhang, W. Xu, *Adv. Energy Mater.* **2018**, 8, 1703022; b) X. Fan, L. Chen, X. Ji, T. Deng, S. Hou, J. Chen, J. Zheng, F. Wang, J. Jiang, K. Xu, C. Wang, *Chem* **2018**, 4, 174; c) D. Xu, J. Su, J. Jin, C. Sun, Y. Ruan, C. Chen, Z. Wen, *Adv. Energy Mater.* **2019**, 9, 1900611; d) Z. Wang, F. Qi, L. Yin, Y. Shi, C. Sun, B. An, H.-M. Cheng, F. Li, *Adv. Energy Mater.* **2020**, 10, 1903843.
- [9] a) X.-Q. Zhang, X.-B. Cheng, X. Chen, C. Yan, Q. Zhang, *Adv. Funct. Mater.* **2017**, 27, 1605989; b) X. Fan, L. Chen, O. Borodin, X. Ji, J. Chen, S. Hou, T. Deng, J. Zheng, C. Yang, S.-C. Liou, K. Amine, K. Xu, C. Wang, *Nat. Nanotechnol.* **2018**, 13, 715; c) L. Lin, F. Liang, K. Zhang, H. Mao, J. Yang, Y. Qian, *J. Mater. Chem. A* **2018**, 6, 15859.
- [10] a) S. Choudhury, Z. Tu, S. Stalin, D. Vu, K. Fawole, D. Gunceler, R. Sundaraman, L. A. Archer, *Angew. Chem., Int. Ed.* **2017**, 56, 13070; b) B. Han, D. Xu, S.-S. Chi, D. He, Z. Zhang, L. Du, M. Gu, C. Wang, H. Meng, K. Xu, Z. Zheng, Y. Deng, *Adv. Mater.* **2020**, 32, 2004793.
- [11] a) A. Kushima, K. P. So, C. Su, P. Bai, N. Kuriyama, T. Maebashi, Y. Fujiwara, M. Z. Bazant, J. Li, *Nano Energy* **2017**, 32, 271; b) S. Li, M. Jiang, Y. Xie, H. Xu, J. Jia, J. Li, *Adv. Mater.* **2018**, 30, 1706375; c) C. Fang, J. Li, M. Zhang, Y. Zhang, F. Yang, J. Z. Lee, M.-H. Lee, J. Alvarado, M. A. Schroeder, Y. Yang, B. Lu, N. Williams, M. Ceja, L. Yang, M. Cai, J. Gu, K. Xu, X. Wang, Y. S. Meng, *Nature* **2019**, 572, 511.
- [12] a) S. S. Zhang, *ACS Appl. Energy Mater.* **2018**, 1, 910; b) S. Nanda, A. Gupta, A. Manthiram, *Adv. Energy Mater.* **2018**, 8, 1801556; c) K.-H. Chen, A. J. Sanchez, E. Kazyak, A. L. Davis, N. P. Dasgupta, *Adv. Energy Mater.* **2019**, 9, 1802534.
- [13] a) Y. Chong, X.-B. Cheng, Y. Yao, X. Shen, B.-Q. Li, W.-J. Li, R. Zhang, J.-Q. Huang, H. Li, Q. Zhang, *Adv. Mater.* **2018**, 30, 1804461; b) R. Xu, X. Zhang, X. Cheng, H. Peng, C. Zhao, C. Yan, J. Huang, *Adv. Funct. Mater.* **2018**, 28, 1705838; c) H. Chen, A. Pei, D. Lin, J. Xie, A. Yang, J. Xu, K. Lin, J. Wang, H. Wang, D. Boyle, Y. Cui, *Adv. Energy Mater.* **2019**, 9, 1900858.
- [14] a) K. C. Möller, T. Hodal, W. K. Appel, M. Winter, J. O. Besenhard, *J. Power Sources* **2001**, 97–98, 595; b) L. Suo, Y.-S. Hu, H. Li, M. Armand, L. Chen, *Nat. Commun.* **2013**, 4, 1481.
- [15] a) D. Aurbach, A. Zaban, A. Schechter, Y. Ein-Eli, E. Zinigrad, B. Markovsky, *J. Electrochem. Soc.* **1995**, 142, 2873; b) E. Peled, D. Golodnitsky, G. Ardel, *J. Electrochem. Soc.* **1997**, 144, L208; c) J.-I. Yamaki, I. Yamazaki, M. Egashira, S. Okada, *J. Power Sources* **2001**, 102, 288; d) Y.-C. Yen, S.-C. Chao, H.-C. Wu, N.-L. Wu, *J. Electrochem. Soc.* **2009**, 156, A95; e) X.-B. Cheng, R. Zhang, C.-Z. Zhao, F. Wei, J.-G. Zhang, Q. Zhang, *Adv. Sci.* **2016**, 3, 1500213; f) X. Yu, A. Manthiram, *Energy Environ. Sci.* **2018**, 11, 527.
- [16] R. Qiao, I. T. Lucas, A. Karim, J. Syzdek, X. Liu, W. Chen, K. Persson, R. Kostecki, W. Yang, *Adv. Mater. Interfaces* **2014**, 1, 1300115.
- [17] B. D. Adams, J. Zheng, X. Ren, W. Xu, J.-G. Zhang, *Adv. Energy Mater.* **2018**, 8, 1702097.